Forecasting Convective Downburst Potential Using GOES Sounder Derived Products

Page 1– Welcome: the lesson you are attending is "Forecasting Convective Downburst Potential Using GOES Sounder Derived Products".

Page 2- The objective of this lesson is to provide a better understanding of the physical processes of downburst generation and the techniques that can be used to nowcast downburst potential using GOES sounder products.

Page 3- This lesson will focus on the physics of downburst generation through a detailed description of the GOES microburst products. The learned concepts will be applied in the prediction exercises based on cases of significant downburst events.

Page 4- You may be familiar with the definition of a downburst as presented in published literature by Fujita and his colleagues. It is important to understand that a downburst consists of two components: the intense convective storm downdraft and the resulting outward "burst" of strong winds on the surface.

Page 5- Pay attention to the "normal" landing path of an aircraft. In the case of a microburst, an aircraft will typically encounter a headwind that serves to slow and lift the nose of the aircraft above the normal landing path. A pilot may compensate for this condition by lowering the nose of the aircraft as it approaches the center of the downdraft core.
Question: What problems may the pilot encounter by taking such a compensating action?

Page 6- "A stationary microburst descends to the ground in its contact stage. As the cold air brought down by the microburst accumulates on the ground, a cushion of the cold air prevents the descending air from reaching the surface. As a result, the height of the extreme wind above the ground increases with time. Meanwhile, the intensity of the extreme wind decreases as the spreading depth increases. A traveling microburst, on the contrary, keeps descending in advance of the cold air which is left behind to form a mesoscale pressure dome. It is likely that the slanted surface of the cold air deflects the outburst winds forward." From Fujita (1981). Thus, a convective storm with forward motion sustains the intensity of the downburst and resulting outflow winds.

Page 7- Studies of two wind-shear-related crashes that occurred in 1975 have shown that the accidents were caused by the aircraft encountering concentrated thunderstorm downdrafts (Caracena et al. 2009). Fujita's analysis revealed for both the Eastern Flight 66 crash at J.F. K. Airport in June and the crash of Continental Flight 469 at Stapleton Airport, Denver, in August, a strong concentrated downdraft along the landing approach very near the crash site. Also studied extensively were microburst-related plane crashes at New Orleans and Dallas-Fort Worth International Airports in 1982 and 1985, respectively. These aircraft disasters prompted a wealth of research in microbursts and the development of techniques to anticipate microburst risk. Ellrod et al. (2000) noted that between 1975 and 1994, 21 fatal downburst-related aircraft accidents were

documented by the National Transportation Safety Board (NTSB). Since 2000, the NTSB has documented ten downburst-related fatal aircraft accidents, mostly involving general aviation flights in the continental United States.

Page 8- Over the past decade there have been a number of marine accidents related to downburst activity. The three most significant disasters include:
- 14 May 1986: The SV Pride of Baltimore, returning from the Caribbean, in what the United States Coast Guard later described as a microburst squall, possibly a white squall, 250 nautical miles (463 km) north of Puerto Rico with winds of 80 knots (150 km/h; 92 mph), capsized and sank. The captain and three crew members died.
- 6 March 2004: the "Lady D", a water taxi servicing the Baltimore Harbor, was capsized in a strong downburst, resulting in five deaths.
- 17 February 2010: the Canadian Sailing Vessel (SV) Concordia capsized and sank off the coast of Brazil due to strong convective storm-generated winds. The SV Concordia was capsized in a downburst that occurred near 1722 UTC, about 290 nautical miles south-southeast of Rio de Janeiro (Capt. William Curry, SV Concordia, personal communication). Amazingly, all 64 of the passengers on board, including crew, faculty, and students, survived the overturning and sinking of the ship.

More recently, during the morning of 25 April 2015, a cluster of thunderstorms developed into a mesoscale convective system (MCS) over eastern Texas and then tracked rapidly eastward along the Gulf of Mexico coast. The MCS intensified rapidly over southern Mississippi and Alabama during the mid-afternoon as the system encountered a very unstable air mass. A large storm cell embedded in the MCS produced a severe downburst over the Mobile Bay during the Dauphin Island Regatta (sailboat race) that resulted in the capsizing and sinking of eight sailing vessels and six deaths. Boat in the image on the right is the "Sweet Louise" that eventually capsized and sank during the storm, but, fortunately resulted in no deaths. Video taken by Joshua Edwards from the SV St. Somewhere:
https://www.youtube.com/watch?v=dJF7i5z9lQ4&feature=player_embedded

Page 9- Accordingly, products derived from the GOES sounder have been developed to assess microburst risk in forecast operations. These are diagnostic indices that are designed to infer differing attributes of microburst environments.

Page 10- The terms "downburst" and "microburst" are used interchangeably in literature and in the media. A microburst is simply a very small downburst with duration of less than five minutes and outflow size of less than five kilometers.

Page 11- GOES sounder-derived microburst products update on the WWW approximately 50 minutes after each sounder scan that occurs on the top of each hour (:00). The products are available in near real-time at the following web address.

Page 12- The GOES microburst product algorithms are based strictly on the thermodynamic structure of the ambient atmosphere and do not incorporate data pertaining to the atmospheric wind profile.

Page 13- The microburst products are designed for use with quasi-stationary, pulse-type convective storms. When applying the microburst products to nowcast downburst potential with larger-scale, migratory convective storm systems, it is important to account for the translational motion of the storms of interest in predicting wind gust potential.

One apparent challenge in the application of the MWPI product over humid regions is the influence of precipitation phase and particle size distribution in a convective storm. The MWPI formula does not explicitly account for precipitation phase or particle size distribution, and thus, in some cases, will either overestimate or underestimate wind gust potential depending on the concentration and particle size distribution of ice-phase precipitation (Strivastava 1987). Convective storms with a core of graupel and hail near the melting level detectable by polarimetric Doppler radar show a tendency for stronger downbursts in which the resulting measured wind gust speeds are closer to the predicted value derived from the MWPI.

The MWPI in some cases overestimates wind gust potential most likely due to the lack of graupel and hail in the storm. This result compliments the finding of Srivastava (1987) that attributes stronger downburst windspeed to the presence of ice (especially hail) in mid-latitude, warm season convective storms. A scenario for MWPI underestimation would result from a convective storm with a precipitation core composed of a high concentration of smaller ice particles. Srivastava (1987) found that a particle size distribution consisting of a high concentration of smaller particles, both ice and liquid, further enhances downdraft intensity and noted that in the case of two storms with similar precipitation content, the storm with a higher concentration of smaller particles will produce a stronger downdraft.

Another challenge to the MWPI used in a downburst forecasting technique is the lower tropospheric environmental moisture (or relative humidity) profile in proximity to a convective storm of interest. Srivastava (1985) noted that lower environmental relative humidity in the boundary layer, a condition typically associated with an "inverted V" thermodynamic profile, has a detrimental effect on downdraft intensity due to the lowering of virtual temperature and the resultant decrease in the virtual temperature deficit between the evaporatively-cooled downdraft and the surrounding environment. Thus, in regions where the "inverted V" thermodynamic profile is favored, such as the U.S. High Plains, a very large ΔDD value will elevate the MWPI, while the environmental virtual temperature in the boundary layer is reduced. The resulting diminished virtual temperature difference between the downdraft and environment will reduce the negative buoyancy of the downdraft and the subsequent downdraft intensity. This condition often results observed downburst-related wind speeds on the surface that are lower than anticipated by the MWPI wind gust prediction algorithm. The dataset employed in the Oklahoma downburst study presented in Pryor (2010) did reveal that the strongest recorded wind gusts (> 25 m s^{-1}) were associated with small to moderate ΔDD values between 2 and 12 K. Larger ΔDD values (> 15 K) often resulted in weaker downburst-related wind gusts of 20 m s^{-1} or less.

Page 14- Wakimoto (1985) defines a wet microburst as a microburst that is accompanied by heavy rain between the onset and the end of high winds. As illustrated by the photograph of a wet microburst on the right, this type is usually associated with intense rain shafts from deep convective storms. The prototype wet microburst environment sounding (Atkins and Wakimoto 1991) is shown on the left. Characteristic of a wet microburst environment is a deep low to mid-tropospheric moist layer.
Question: Based on the sounding profile and photograph, if you were to develop a wet microburst index product, what relevant parameters would you include?

Page 15- The WMSI algorithm summarizes microburst windspeed potential by considering the most relevant parameters for downdraft generation. Large amounts of positive buoyant energy (PBE) or convective available potential energy (a.k.a. CAPE) typically results in the generation of high precipitation content within a convective storm cell. Moisture stratification, best expressed as a vertical difference or gradient in equivalent potential temperature (θ_e), is important to consider in locating and identifying a source of mid-tropospheric dry air that can be ingested into the storm precipitation core. Loading of heavy precipitation and the mid-level dry air play an important role in downdraft initiation and acceleration.

Page 16- As stated in the previous slide, the vertical equivalent potential temperature (θ_e) profile can provide useful information pertaining to wet microburst environments. Atkins and Wakimoto (1991) found that a significant difference in θ_e between the surface and mid-troposphere, typically greater than 20 K, was associated with wet microbursts that occurred in northern Alabama during the 1986 Microburst and Severe Thunderstorm (MIST) project.

Page 17- This is an example of a local scale GOES-13 microburst product image over the Jacksonville, Florida area at 1945 UTC 10 June 2014. Colored contours of MWPI values are overlying MWPI values (plotted in yellow type) and $\Delta\theta_e$ values (plotted in blue type). Compare to the Rapid Refresh (RAP) model-derived theta-e profile at the same time (right) over Jacksonville, very similar to the prototype profile in the previous slide, that shows a prominent dry-air layer near altitude 3,000 meters AGL (near 700-mb level). At 2150 UTC, a wind gust of 25 m s^{-1} (48 kt) was recorded at Whitehouse Naval Outlying Field ("NEN") and confirmed as resulting from a downburst.

Page 18- More recently, James and Markowski (2010), based on numerical simulations, found that dry air aloft had a detrimental effect on convective intensity that resulted in a reduction in hydrometeor mass, especially a decrease in hail generation. The reduced hail mixing ratio and resulting reduction in hail melting rate was a factor in the offset of the favorable effects of dry air aloft for downdraft development. The overall effect of dry air aloft was to reduce downdraft mass flux and cold pool strength in low-to-moderate CAPE environments. Complementary to the results of James and Markowski (2010), a poor correlation between $\Delta\theta_e$ and downburst magnitude will be shown

Page 19- Since both virtual temperature and θ_e are proportional to moisture content (mixing ratio) of the environment, higher relative humidity in the boundary layer often

results in an elevated virtual temperature and θ_e. Thus, in addition to indicating the presence of a mid-tropospheric unsaturated air layer, large $\Delta\theta_e$ values signify the presence of elevated boundary layer relative humidity as compared to higher layers in the troposphere. Therefore, in the situation where environmental virtual temperature is elevated due to higher relative humidity, the virtual temperature deficit between the downdraft and the environment is often increased, resulting in enhanced downdraft intensity.

Page 20- This page summarizes the most important components of the microburst physical process. The CAPE term represents the process of updraft generation and resulting precipitation loading. The TeD term represents the process of negative buoyancy generation that results from the entrainment of dry air into the precipitation core.

Page 21- RAP model analysis sounding thermodynamic profile over Whitehouse Field (NEN), Jacksonville, Florida, at 2000 UTC 10 June 2014 (left). The dashed curve in thermodynamic profile represents virtual temperature. "ML" marks the height of the melting level (273 K or 0° C isotherm). CAPE, represented by the shaded area, is in units of J kg^{-1}. The RAP model-derived sounding profile (left) and photograph of a downburst-producing convective storm (right) summarize the wet microburst environment in which high WMSI values indicate that the ambient sounding profile "fits", to a large degree, the prototypical wet microburst profile.

Page 22- Wakimoto (1985) defines a dry microburst as a microburst that is accompanied by little or no rainfall between the onset and the end of high winds. As illustrated by the photograph of a dry microburst on the right, this type is usually associated with virga from shallow, high-based cumulonimbus clouds. The prototype dry microburst environment sounding is shown on the left. Characteristic of a dry microburst environment is a deep, dry sub-cloud layer associated with an "inverted V" sounding profile.
Question: Based on the sounding profile and photograph, if you were to develop a dry microburst index product, what relevant parameters would you include?

Page 23- The Dry Microburst Index (DMI) algorithm stands in contrast to the WMSI as it considers relevant parameters in the deep, dry subcloud layer typically found over the western U.S. The steep, dry-adiabatic temperature lapse rate and large vertical relative humidity gradient, expressed as a dewpoint depression difference, foster downdraft acceleration as precipitation evaporates in the subcloud layer.

Page 24- GFS model thermodynamic profile over Bankura, India at 0900 UTC 3 May 2015 (left); Figure 20 from Ellrod (1989): VAS sounding at DFW interpolated from retrievals 248 and 276 at 2218 UTC 2 August 1985, showing the area of positive buoyant energy (PBE), total negative buoyant energy (NBE), the level of free convection (LFC) and the equilibrium level (EL).
Hybrid microburst sounding profile features characteristics of both wet and dry microburst environments and is typical for Great Plains region during the warm season.
Attributes include:
Large positive area/CAPE.

Little or no capping inversion.
A dry adiabatic lapse rate layer, at least 5000 ft deep.
A moist mid-tropospheric layer.
These sounding characteristics indicate an intermediate microburst environment in which sub-cloud evaporation of precipitation is still a major factor in microburst generation, even though the parent storm may produce heavy rain. (Caracena et al. 2009).

Page 25- The GOES MWPI algorithm combines the most important elements of the wet and dry microburst assessment process and thus, can more effectively assess downburst wind gust potential over most of the central and western U.S.

Page 26- An MWPI product image that displays an area of convective storms developing along the south Florida sea breeze convergence zone. Note elevated MWPI values (>40) over northeastern Florida, indicating downburst wind gust potential of 20 m s^{-1} (40 kt) or greater, that persisted in the vicinity of the sea breeze front through the afternoon. During the period of 1800 to 2100 UTC, two bands of enhanced cumulus clouds merged over the city of Jacksonville while intense deep convection that developed over east-central Florida was spreading northward. Outflow boundary interaction with the sea breeze front and the subsequent merger of a cluster of thunderstorms over the western portion of the city of Jacksonville during the late afternoon resulted in the development of a large, high-reflectivity thunderstorm that would eventually produce a strong downburst at Whitehouse Naval Outlying Field. At 2150 UTC, a wind gust of 25 m s^{-1} (48 kt) was recorded at Whitehouse Naval Outlying Field and confirmed as resulting from a downburst.

Page 27- This is an example of a Western U.S. sector MWPI product image that displays widespread convective storm activity developing over the Great Basin and Rocky Mountain regions. Note elevated index values (yellow) over most of Utah. Downburst wind gusts of 40 to 67 knots occurred over Dugway Proving Ground, Utah, southwest of the Great Salt Lake, between 2100 and 2300 UTC 10 June 2014.

Page 28- RAOB sounding profile over Salt Lake City, Utah at 0000 UTC 13 June 2013. This profile is associated with an MWPI value of 27 and a downburst wind gust of 65 knots measured at Salt Lake City Municipal Airport (U42) at 0027 UTC.

Page 29- The primary differences between the respective microburst environments discussed to this point are the relative depth and location of moist and dry layers and the presence of CAPE. Common for all microbursts is the dominance of evaporational cooling in the generation of negative buoyancy and downdraft acceleration.

Page 30- In 1994, McCann developed a microburst prediction algorithm that produces an assessment of wind gust potential. The output of the Wind Index (WINDEX) algorithm is an expected convective wind gust speed in knots.

Page 31- Similar to the previously discussed products, The WINDEX is built upon physically relevant parameters for downburst generation. Strong dependence of the

WINDEX algorithm on the temperature lapse rate may yield unrepresentatively low index values in nocturnal inversion conditions.

Page 32- This is an example of a GOES sounder-derived WINDEX product image on 10 June 2014 in which index values are plotted at retrieval locations on visible satellite imagery. Downburst wind gusts of 40 to 67 knots occurred over Dugway Proving Ground, Utah, southwest of the Great Salt Lake, between 2100 and 2300 UTC 10 June 2014.

Page 33- This graphic is an example of product validation results from the past several years. Validation based on 208 downburst events over Oklahoma and western Texas between 2007 and 2010 convective seasons indicated a strong correlation between MWPI values and observed surface convective wind gusts. The scatterplot of MWPI values versus observed downburst wind gust speed as recorded by mesonet stations in Oklahoma and Texas identifies two clusters of values: MWPI values less than 50 that correspond to observed wind gusts of 35 to 50 knots, and MWPI values greater than 50 that correspond to observed wind gusts of greater than 50 knots. The scatterplot illustrates the effectiveness of the MWPI product in distinguishing between severe and non-severe convective wind gust potential.

Page 34- Now we will apply the concepts learned in this lesson to recent significant cases of downburst events. These exercises will give you the opportunity to apply the GOES microburst products in operational forecasting situations.

Case 1: During the afternoon of 10 August 2009, strong convective storms developed along a cold front that extended from eastern Kansas to the Oklahoma Panhandle. The storms tracked eastward and produced several strong downbursts over northwestern and north-central Oklahoma during the late afternoon and evening. Table 1 features a listing of five significant high wind measurements by Oklahoma Mesonet stations during this downburst event. The last and highest downburst wind gust of the event, 33 ms^{-1} (64 kt), was recorded at Freedom station at 2345 UTC.

Table 1. Measured wind gusts compared to MWPI values and OT properties for the 10 August 2009 Oklahoma downburst event. All times are in UTC.

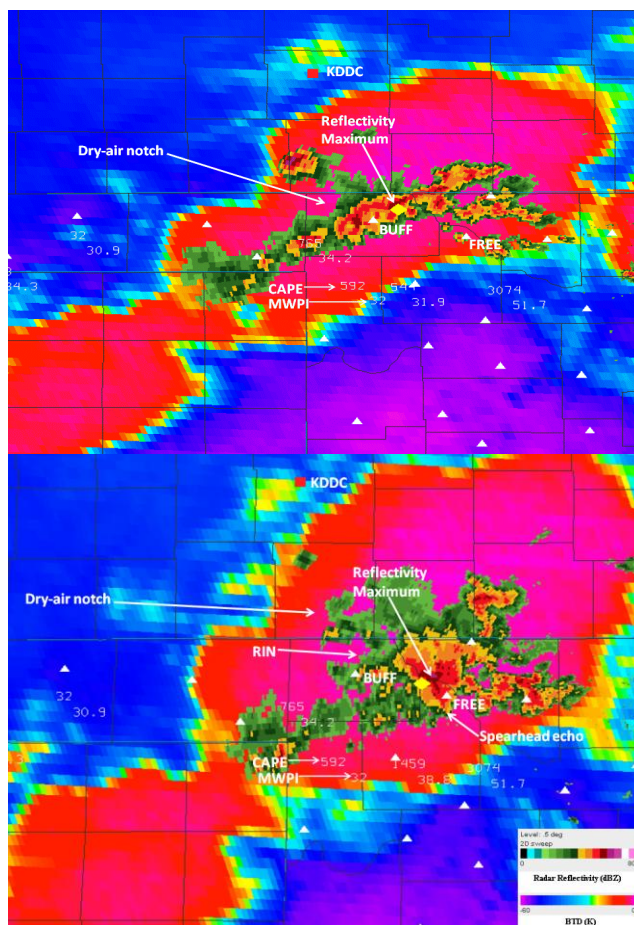| Time	Gust Speed ms^{-1} (kt)	Location	MWPI	OT Time	OT Dist (km)	OT Min (°K)	OT Mag (°K)
2115	20.6 (40)	Copan	31	2115	9	206.5	-9.2
2125	22.1 (43)	Lahoma	44	2115	9	210.1	-7
2230	21.1 (41)	Slapout	33	2215	12	211.6	-8.7
2305	23.1 (45)	Buffalo	39	2302	13	203.5	-8
2345	32.9 (64)	Freedom	52	2332	13	196.8	-11.2

Page 35- Oklahoma sector GOES MWPI product image animation between 2000 and 2300 UTC 10 August 2009.

Task: Based on the MWPI animation, identify regions of high downburst risk and associated wind gust potential over the central and southern Great Plains region.

Page 36- Corresponding WMSI product image animation between 2000 and 2200 UTC.

Task: Note any differences in spatial patterns of WMSI values as compared to the MWPI product from the same time period. Modify (if necessary) your assessment based on the WMSI product animation.

Page 37- Below: composite image of GOES MWPI at 2200 UTC, GOES channel 3-4 (WV-IR) BTD at 2302 UTC, and radar reflectivity from Vance AFB NEXRAD at 2305 UTC 10 August 2009 (top) compared to a composite image of GOES MWPI, BTD at 2332 UTC, and radar reflectivity at 2343 UTC (bottom). The overshooting top, as indicated by the Bedka algorithm, is marked with a yellow triangle. The location of the Dodge City RAOB is marked with a red square.

A dry air notch had become especially well-defined on the northwestern flank of a convective storm in phase with a RIN as apparent in radar imagery and shown in the

2302 UTC BTD image. Note that the overshooting top was co-located with a maximum in radar reflectivity and located 13 km northeast of the Buffalo (BUFF) mesonet station, where a downburst wind gust of 23 ms^{-1} (45 kt) was recorded at 2305 UTC. During the next 30 minutes, the multicellular storm intensified as it tracked eastward toward higher CAPE (3074) and MWPI (51.7) values southeast of Freedom (FREE). At 2345 UTC, a much stronger downburst was recorded at Freedom mesonet station. The cold overshooting top BT value of 196°K, located 13 km northwest of Freedom, was associated with the severe downburst, highlighting the importance of convective storm updraft strength in the generation of severe weather, especially high winds. In a similar manner to the previous OT, the OT near Freedom was co-located with a maximum in reflectivity (> 65 dBZ). The closest representative MWPI value of 52 corresponded to wind gust potential of 25 to 33 ms^{-1} (50 to 64 kt). A dry air notch, apparent in the BTD image as a light-to-dark blue shaded indentation, illustrated the role and importance of the entrainment of dry, mid-tropospheric air into the rear flank of the convective storm and the subsequent generation of intense downdrafts. The displacement between the dry-air notch and the RIN identified in radar imagery was likely due to the 11-minute time difference between the satellite and radar images.

Page 38- Dodge City, Kansas (DDC) radiosonde observation (RAOB) at 0000 UTC 11 August 2009. Courtesy of University of Wyoming.

Task- Using pattern recognition and parameter evaluation techniques, identify attributes in the sounding profile that indicate a favorable environment for downbursts.

Case 2: During the morning of 25 April 2015, a cluster of thunderstorms developed into a mesoscale convective system (MCS) over eastern Texas and then tracked rapidly eastward along the Gulf of Mexico coast. The MCS intensified rapidly over southern Mississippi and Alabama during the mid-afternoon as the system encountered a very unstable air mass. A large storm cell embedded in the MCS produced a severe downburst over the Mobile Bay during the Dauphin Island Regatta (sailboat race) that resulted in the capsizing and sinking of several sailing vessels and six deaths.

Page 39- Central Gulf of Mexico coast GOES-13 visible (VIS) image at 1845 and 1945 UTC 25 April 2015 with overlying $\Delta\theta_e$ (blue) and MWPI (yellow) values, and contours of MWPI values with an interval of 10. White triangles mark the location of coastal marine stations in the Mobile Bay.
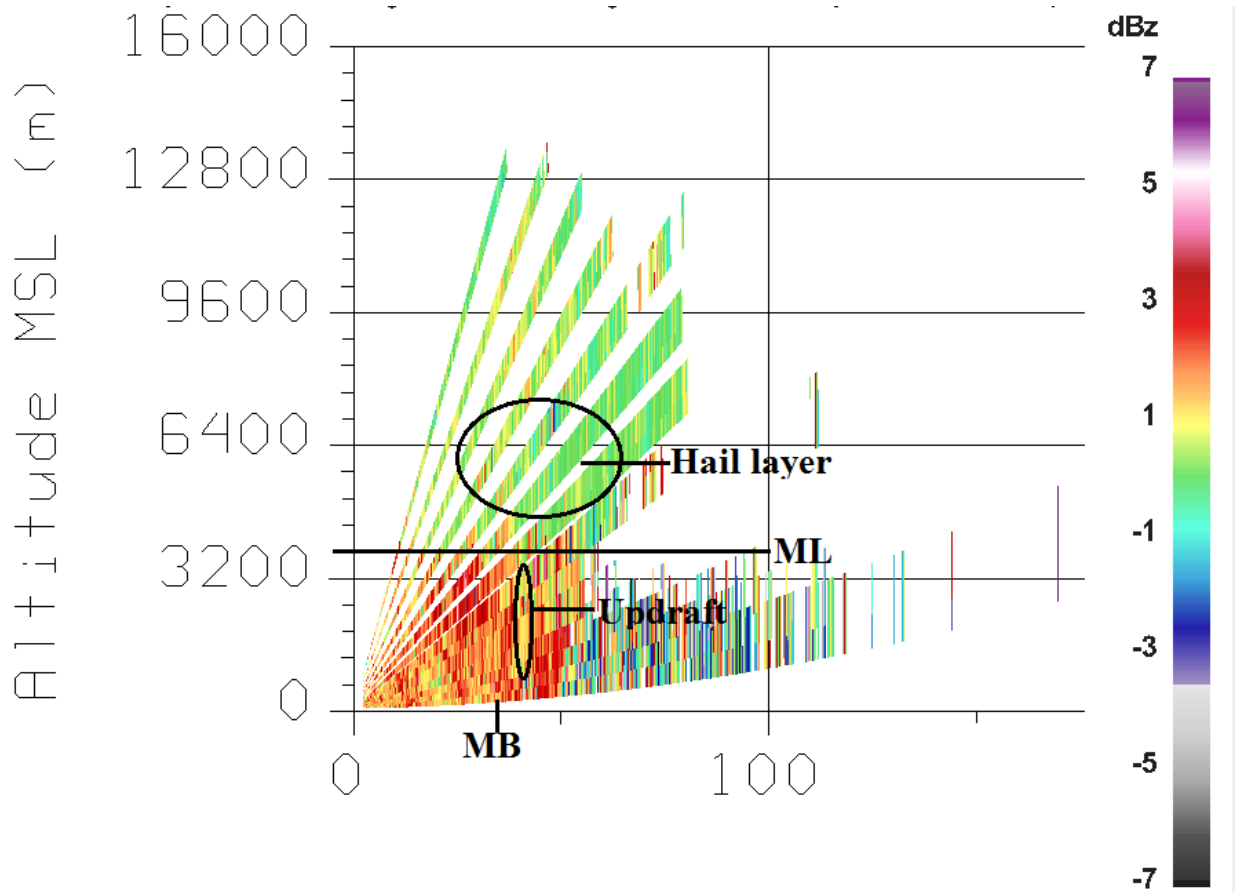
Page 40- Rapid Refresh (RAP) model-derived MWPI at 1900 and 2000 UTC 25 April 2015, with overlying radar reflectivity from Mobile, Alabama NEXRAD.

Task- Based on the GOES and RAP MWPI product imagery on pages 39 and 40, provide reasoning for why the Mobile Bay area was favored for severe downburst winds that impacted the Dauphin Island Regatta between 2000 and 2100 UTC.

Page 41- Mobile Bay region RAP model-derived MWPI at 2000 UTC with overlying radar reflectivity from Mobile, Alabama NEXRAD between 2000 and 2024 UTC.

Task- What radar signatures can you identify that are associated with downburst occurrence?
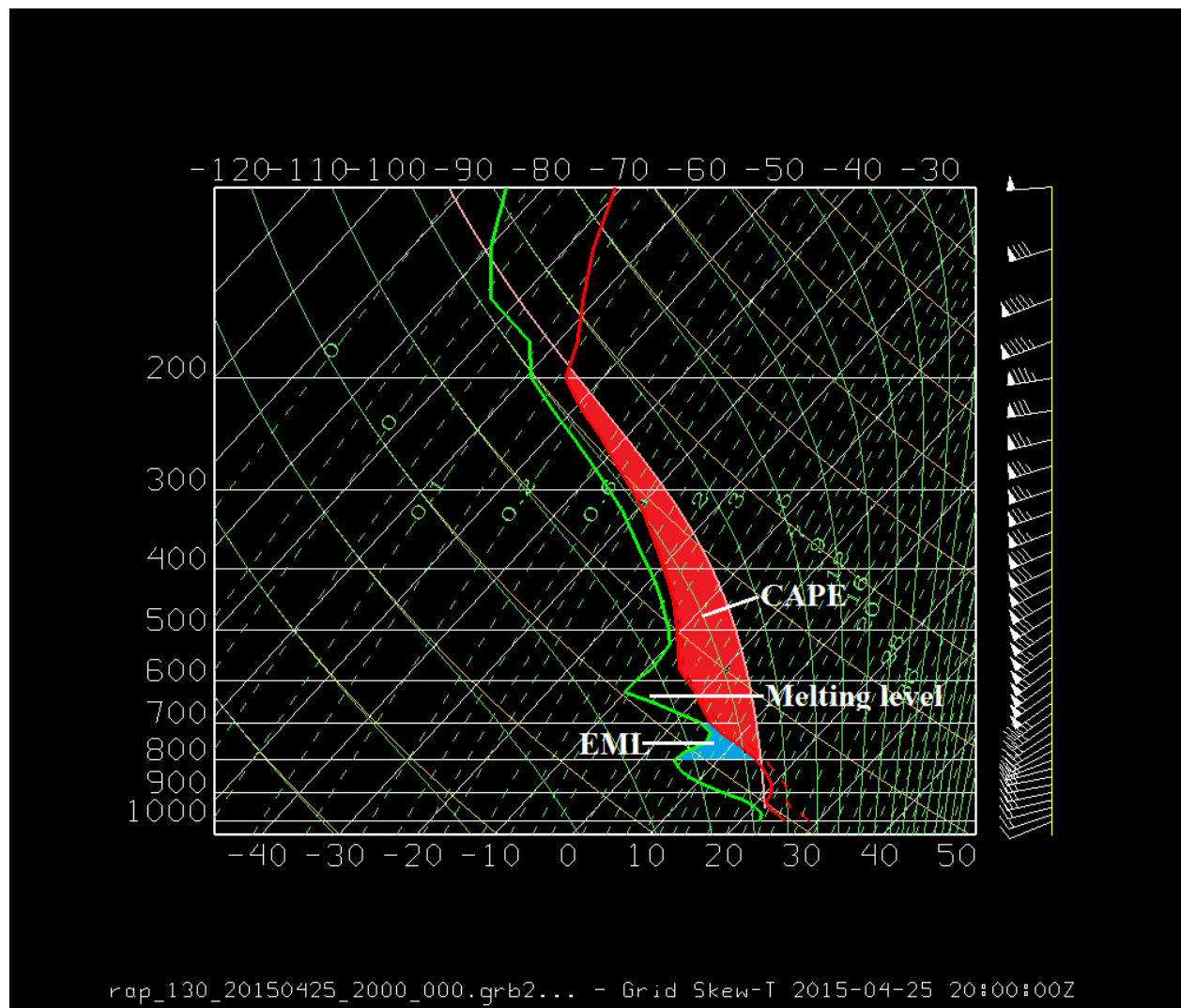
Page 42- Mobile, Alabama differential reflectivity (ZDR) range height indicator (RHI) imagery between 2008 and 2019 UTC 25 April 2015.

Mobile, Alabama differential reflectivity (ZDR) range height indicator (RHI) image at 2014 UTC 25 April 2015. "MB" marks the location of Middle Bay Lighthouse. "ML" marks the height of the melting level as identified in a thermodynamic profile over the Mobile Bay at 2000 UTC. Horizontal distance scale is in kilometers (km).

Task- What ZDR signatures can you identify that are associated with downburst occurrence?

Page 43- RAP model thermodynamic profiles over Mobile Bay at 1900 and 2000 UTC 25 April.

RAP model thermodynamic profile over Mobile Bay at 2000 UTC 25 April.

Task- Using pattern recognition and parameter evaluation techniques, identify attributes in the sounding profile that indicate a favorable environment for downbursts.

Page 44- $\Delta\theta_e$ profile over Mobile Bay at 1900 and 2000 UTC 25 April.

Task- Estimate $\Delta\theta_e$ for each profile and discuss how the profile contributes to downdraft severity.

Case 3: During the afternoon of 6 July 2014, a plume of mid-tropospheric moisture was well-established over the southwestern U.S. associated with the development of the North American Monsoon. Moist, easterly mid-tropospheric flow along the southern periphery of the subtropical high pressure ridge and intense solar heating of the surface, especially mountain slopes, resulted in the development of orographic convective storms during the afternoon hours over New Mexico, Arizona and Utah. By late afternoon (2200 UTC), new convective storms initiated over the Utah-Nevada border along an outflow boundary

generated by earlier thunderstorm activity over southwestern Utah. Over the next several hours, this cluster of thunderstorms would track westward and southwestward over southern Nevada near Las Vegas and produce numerous severe downbursts over the Nevada National Security Site (NNSS). Peak wind gusts recorded at the NNSS are listed in Table 1.

Page 45- Western U.S. sector GOES MWPI product animation during the evening of 6 July 2014 (0000 to 0200 UTC 7 July) showing high risk values (>50, red) in place over southeastern Nevada as the thunderstorm complex was tracking westward and southwestward toward the California-Nevada border.

Task: Based on the MWPI animation, identify regions of high microburst risk over the southwestern U.S.

Page 46- Southwestern U.S. sector GOES MWPI product animation during the evening of 6 July 2014 (2300 to 0200 UTC 7 July) showing high risk values (>50, red) in place over southeastern Nevada as the thunderstorm complex was tracking westward and southwestward toward the California-Nevada border.

Task: Based on the MWPI animation, identify regions of high microburst risk over the southwestern U.S.

Page 47- GOES Wind Index (WINDEX) southwestern U.S. sector product animation during the evening of 6 July 2014. Note values greater than 50 knots persisting over southern Nevada downstream of the thunderstorm complex.

Task: Note any differences in spatial patterns of WINDEX values as compared to the MWPI product from the same time period. Modify (if necessary) your assessment based on the WINDEX product animation.

Page 48- RAP model-derived sounding profile animation at the NNSS between 0000 and 0200 UTC 7 July 2014. The animation shows a persistent "inverted-V" profile with a general increase in CAPE during the two hour period prior to downburst occurrence over NNSS. The inverted-V profile signifies the persistence of a deep, well-mixed convective boundary layer that was favorable for the generation of intense storm downdrafts as precipitation melted and evaporated in the subcloud layer.

Task- Using pattern recognition and parameter evaluation techniques, identify attributes in the sounding profile that indicate a favorable environment for downbursts.

Page 49- GOES-15 WV-IR BTD-NEXRAD composite image animation from 0241 to 0330 UTC 7 July 2014 showing an overview of the evolution of a thunderstorm complex tracking westward over southern Nevada. Las Vegas NEXRAD displayed spearhead echoes, with high reflectivities, associated with downburst occurrence over the NNSS. Downburst wind gusts between 59 and 62 mph (51 to 54 knots) were recorded by NNSS mesonet stations.

Station	Peak Wind Gust (knots)	Time (UTC)
A43	52	0245
A27	54	0300
A23	51	0315
A30	52	0315

Table 1. Downburst wind gusts recorded by ARL SORD mesonet stations at the Nevada National Security Site on 7 July 2014.

Page 50- Future work: Application and validation of downburst potential products over diverse geographic and climate regions (i.e. western Unites States, Florida, India)
- NOAA Technical Report NESDIS 140 :
  - http://www.star.nesdis.noaa.gov/star/documents/bios/Pryor_K/nesdistechr pt140.pdf
- SPIE conference paper:
  - http://proceedings.spiedigitallibrary.org/proceeding.aspx?/proceeding.aspx ?articleid=1935145&articleid=1935145

Page 51-53- References used in the development of this lesson. Please feel free to review these references for more background pertaining to microbursts and the GOES products.

References

Atkins, N.T., and R.M. Wakimoto, 1991: Wet microburst activity over the southeastern United States: Implications for forecasting. *Wea. Forecasting*, **6**, 470-482.

Caracena, F., and J.A. Flueck, 1988: Classifying and forecasting microburst activity in the Denver area. *J. Aircraft*, **25**, 525-530.

Caracena, F., R.L. Holle, and C.A. Doswell, cited 2009: Microbursts-A handbook for visual identification. Available online at http://www.cimms.ou.edu/~doswell/microbursts/Handbook.html.

Doswell, C.A., 2001: Severe convective storms- An overview. *Severe Convective Storms*, C.A. Doswell, Ed., Amer. Meteor. Soc., 1-26.

Ellrod, G. P., 1989: Environmental conditions associated with the Dallas microburst storm determined from satellite soundings. *Wea. Forecasting*, **4**, 469-484.

Ellrod, G.P., J.P. Nelson, M.R. Witiw, L. Bottos, and W.P. Roeder, 2000: Experimental GOES sounder products for the assessment of downburst potential. *Wea. Forecasting*, **15**, 527-542.

Fujita, T.T., 1981: Tornadoes and downbursts in the context of generalized planetary scales. *J. Atmos. Sci.,* **38,** 1511–1534.

Fujita, T.T., and R.M. Wakimoto, 1983: Microbursts in JAWS depicted by Doppler radars, PAM and aerial photographs. Preprints, *21st Conf. on Radar Meteorology*, Edmonton, Amer. Meteor. Soc., 638-645.

James, R. P., and P. M. Markowski, 2010: A numerical investigation of the effects of dry air aloft on deep convection. *Mon. Wea. Rev.*, **138**, 140–161.

McCann, D.W., 1994: WINDEX-A new index for forecasting microburst potential. *Wea. Forecasting*, **9**, 532-541.

Pryor, K. L., 2010: Recent developments in microburst nowcasting using GOES. *17th Conf. on Satellite Meteorology and Oceanography*, Annapolis, MD, Amer. Meteor. Soc., P9.7. [Available online at https://ams.confex.com/ams/17Air17Sat9Coas/webprogram/Paper174313.html]

Pryor, K.L., 2011: Microburst Nowcasting Applications of GOES. NOAA Technical Report NESDIS 140.

Pryor, K.L., 2012: Microburst Nowcasting Applications of GOES. 18th *Conf. on Satellite Meteorology and Oceanography*, New Orleans, LA, Amer. Meteor. Soc.

Pryor, K. L., 2014: Downburst prediction applications of meteorological geostationary satellites. *Proc. SPIE Conf. on Remote Sensing of the Atmosphere, Clouds, and Precipitation V*, Beijing, China, doi:10.1117/12.2069283.

Srivastava, R. C., 1985: A simple model of evaporatively driven downdraft: Application to microburst downdraft. *J. Atmos. Sci.*, **42**, 1004-1023.

Srivastava, R. C., 1987: A model of intense downdrafts driven by the melting and evaporation of precipitation. *J. Atmos. Sci.*, **44**, 1752-1773.

Wakimoto, R.M., 1985: Forecasting dry microburst activity over the high plains. *Mon. Wea. Rev.*, **113**, 1131-1143.

Wakimoto, R.M., 2001: Convectively Driven High Wind Events. *Severe Convective Storms*, C.A. Doswell, Ed., Amer. Meteor. Soc., 255-298.